ACS APPLIED MATERIALS & INTERFACES

Research Article

www.acsami.org

Selective Detection of Volatile Organic Compounds by Spectral Imaging of Porphyrin Derivatives Bound to TiO_2 Porous Films

Javier Roales,[†] José M. Pedrosa,*[,†] Pedro Castillero,[†,‡] Manuel Cano,[†] Tim H. Richardson,[§] Ángel Barranco,[‡] and Agustín R. González-Elipe[‡]

[†]Departamento de Sistemas Físicos, Químicos y Naturales, Universidad Pablo de Olavide, Ctra. Utrera Km. 1, 41013 Sevilla, Spain
[§]Department of Physics and Astronomy, University of Sheffield, Hicks Building, Hounsfield Road, Sheffield S37RH, United Kingdom
[‡]Instituto de Ciencia de Materiales de Sevilla, Universidad de Sevilla−CSIC, Américo Vespucio 49, 41092, Sevilla, Spain

Supporting Information

ABSTRACT: In this work, the carboxylic acid derivatives of a free-base porphyrin, 5,10,15,20-tetrakis(4-carboxyphenyl)-21*H*,23*H*-porphyrin, and 10 of its metal derivatives (TCPPs) have been used for optical gas sensing. For this purpose, microstructured columnar TiO_2 thin films prepared by GAPVD (glancing angle physical vapor deposition) have been used as host materials for the porphyrins as they are non−dispersive and porous, allowing their use for UV−visible spectroscopy and gas sensing. The chemical binding between the dye molecules and the TiO_2 has been studied through infrared spectroscopy, and the obtained spectral changes have been found to be compatible with chelating and/or bidentate binding modes of the carboxylate groups on the TiO_2 surface. When hosted in the film, the UV−visible spectra of the porphyrins featured a blue shift and broadening of the Soret band with respect to the solution, which has been attributed to the formation of $\pi-\pi$ aggregates between porphyrin molecules. The composite porphyrin/TiO_2 films obtained from each of the 11 porphyrins have been exposed to 12 different volatile organic compounds (VOCs), and their respective gas−sensitive properties have been analyzed as a function of the spectral changes in their Soret band region in the presence of the analytes. The set of composite films has shown high selectivity to the analyzed volatile compounds. For each analyte, an innovative way of showing the different responses has been developed. By means of this procedure, an imagelike recognition pattern has been obtained, which allows an easy identification of every compound. The kinetics of the exposure to several analytes showed a fast, reversible and reproducible response, with response times of a few seconds, which has been attributed to both the sensitivity of the porphyrins and the high porosity of the TiO_2 films. Also, increasing concentrations of the analytes resulted in an increase in the magnitude of the response, indicating that the sensor behavior is also concentration-dependent.

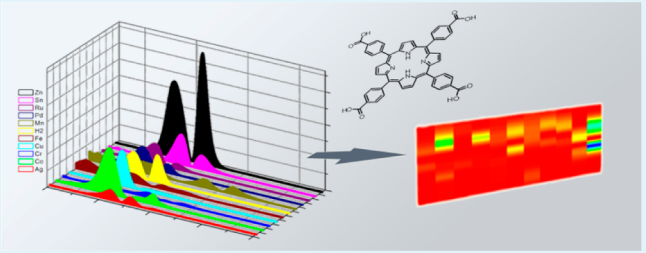

KEYWORDS: *carboxyphenyl porphyrin, TiO_2 nanostructures, volatile organic compounds, optical sensing, spectral imaging, gas sensors*

1. INTRODUCTION

The detection of volatile organic compounds (VOCs) through electronic nose technologies has been generally based on metal-oxide semiconductors and on conducting polymer resistive materials.[1,2] Such systems have shown good results for the discrimination of analytes of different chemical functionality, but the distinction of compounds from within a given chemical class continues to be a challenging task.[3] Also, these materials are not appropriate for the detection of metal-binding species, when many of the most toxic and odorous compounds are excellent ligands for metal ions. Thus, detection of molecules such as amines, phosphines, and thiols has been much less explored.[4]

In the past few years, metalloporphyrins have been employed for the optical detection of different gases.[3−9] These molecules are quite stable and their properties can be precisely tuned by modifications of their molecular structure. The sensing properties of metalloporphyrins depend on the coordinated metal, the peripheral substituents and the conformation of the macrocycle.[10] Also, the organic chemistry of these compounds has been widely investigated, so that there are many synthesis routes describing the introduction of a wide range of substituents at their peripheral positions, and a high number of the metals can be coordinated to the porphyrin core.[10]

The presence of $\pi-\pi$ interactions between porphyrins may cause aggregation when the molecules are deposited on solid substrates, which can result in broadening, shifting and splitting of the bands present in the spectrum with respect to the porphyrin solution.[11] In the case of VOC detection, the interaction with this kind of compound may modify these interactions, resulting in modifications of the spectrum that can be used for sensing applications.[10]

Received: June 5, 2012
Accepted: September 17, 2012
Published: September 17, 2012

   dx.doi.org/10.1021/am3010169 | *ACS Appl. Mater. Interfaces* 2012, 4, 5147−5154

In the search of porphyrin-based sensors, a wide range of substrates can be used as solid support for these molecules, from glass (for example, in the Langmuir−Blodgett technique)[12−14] to silica gel.[3,4] Meanwhile, solar cell researchers have been sensitizing TiO_2 with several organic dyes for light harvesting, and some of them have focused their attention on porphyrins because of their efficacy in photosynthesis. As a result of this, the anchoring to TiO_2 has been studied for a number of functional groups, such as salicilate, sulfonic acid, phosphonic acid, acetylacetonate and one of the most widely used derivatizations, carboxylic acid.[15] However, TiO_2 films prepared for solar cell purposes are usually thick and very dispersive, which makes them inappropriate for gas sensing when using UV−visible spectroscopy.

Recently, the preparation of columnar TiO_2 thin films by physical vapor deposition has been developed.[16] These materials are characterized by a columnar microstructure with large and open pores which makes them very accessible to molecules originating from outside the film.[17] Because of these characteristics, these systems have been found to be ideal for the study of diffusion processes of relatively large molecules such as porphyrins.[18,19] This structure also allows fast diffusion of gaseous analytes which is necessary for the gas sensing application. On the other hand, the columnar TiO_2 films are thin and non dispersive, allowing optical transmission measurements. Therefore, the combination of these structural properties with the possibility of chemical anchoring of the sensing dye, makes the TiO_2 a very good candidate for the fabrication of porphyrin-based sensors. Another good possibility would be the use of ZnO, which easily grows in nanowires and other nanostructures.[20] However, the lack of stability in normal atmosphere and aqueous media is the main disadvantage of this material whose binding mechanism with the dye does not work as well as in TiO_2. Silica[4] and ormosils[21] have been also used as hosting matrices for porphyrin sensors with very nice results. However these materials are not equivalent to TiO_2 in any of their variants since do not allow chemical binding of the dye and therefore do not permit to exploit this particular capability. Finally, TiO_2 (like ZnO) also offers the possibility of using its well-known photonic properties for gas sensing applications. Although the measuring setup becomes more complicated than simple absorption spectroscopy, good sensibilities and selectivity have been found by following photoconductivity changes in the presence of several gas analytes.[22]

In this work, the carboxylic acid derivatives of a free-base porphyrin and 10 of its metal derivatives (TCPPs) have been used for optical gas sensing of volatile organic compounds. For this purpose, microstructured columnar TiO_2 thin films have been used as hosts for the porphyrins and the chemical binding between the porphyrin and the TiO_2 has been confirmed through infrared spectroscopy. Also, the influence of this binding on the porphyrin aggregation and orientation has been investigated. The optical responses of the set of porphyrins to a total of 12 individual VOCs have been analyzed, and the magnitude of the spectral changes has been represented as color image patterns with spectral resolution, which allows selective recognition for each analyte.

2. EXPERIMENTAL SECTION

2.1. Metal Oxide Matrix. Transparent and amorphous TiO_2 films were prepared by the GAPVD (glancing angle physical vapor deposition) technique at room temperature. For UV−visible spectroscopy the films were deposited on glass substrates. For specular reflectance FT−IR spectroscopy, the films were prepared on gold-coated silicon substrates. Gold coating was performed by sputtering onto silicon substrates. Evaporation was carried out by using TiO pellets in the solid state as a target, which were converted into a vapor by bombardment from a high energy electron beam. As the vapor condensed on the surface of the substrate, it forms a thin layer. This process was performed under vacuum conditions at about 1×10^{-4} Torr of O_2 in order to obtain columnar thin films of TiO_2. The deposition onto the substrates was carried out using the GAPVD technique through the use of a home−made sample holder. It consisted of a 40 cm diameter steel circular plate from which the samples were hung in a vertical position. The radial separation between the evaporation center and the sample position provides the different inclinations of the substrates, relative to the direction of evaporation. Through this procedure, five angles of incidence (60, 70, 80, 85, and 90°), measured between the normal to the sample and the incident direction, were obtained.

Films with a thickness in the range 150−400 nm were prepared by this method. The microstructure of these films deposited on a silicon wafer was examined by field emission scanning electron microscopy (FESEM) in a Hitachi S5200 microscope. Cross-sectional views were obtained by cleaving the silicon substrates. A common property of the obtained films is their high porosity and, as a consequence, they exhibit relatively low values of refractive index.

2.2. Porphyrins. A total of 11 porphyrins have been used in this work, one non−metalated and 10 of its metal derivatives. The structure of 5,10,15,20-tetrakis(4-carboxyphenyl)-21*H*,23*H*-porphyrin (H_2TCPP) is shown in Figure 1. In the metal derivatives, the two hydrogen atoms in the center of the porphyrin ring are replaced with the corresponding metal ion (i.e., Ag(II), Co(III), Cu(II), Cr(III), Fe(III), Mn(III), Pd(II), Ru(II), Sn(IV), and Zn(II)). Hereafter, compounds will be named by their metal ion followed by TCPP. All porphyrins were purchased from Frontier Scientific Europe Ltd. and were used without further purification.

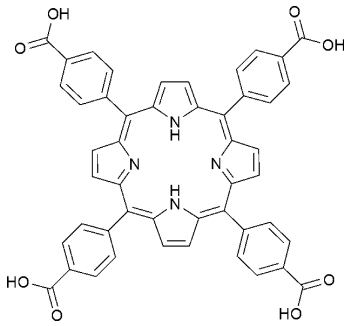

Figure 1. Molecular structure of 5,10,15,20-tetrakis(4-carboxyphenyl)-21*H*,23*H*-porphyrin. In the metal derivatives, the two hydrogen atoms in the center of the porphyrin ring are replaced with Ag(II), Co(III), Cu(II), Cr(III), Fe(III), Mn(III), Pd(II), Ru(II), Sn(IV), or Zn(II).

2.3. Binding. Binding of the dye molecules to the TiO_2 films was carried out by immersing the films in a 10^{-4} M EtOH solution of the dye at room temperature (21 °C) for 1 h. The infiltrated films were rinsed, immersed in EtOH to remove physisorbed dye and then dried using dry N_2 through a nitrogen gun. All films, which were stored in air, were dried by heating to 110 °C for 30 min and allowed to cool to 20 °C under a dry N_2 gas stream prior to the measurements.

2.4. Infrared Spectroscopy. The study of the binding of the carboxylic porphyrins to TiO_2 was performed through specular reflectance Fourier transform infrared (FT−IR) spectroscopy using a Jasco FT/IR−6200 spectrometer. This measuring setup provided us with enough signal for the required analysis in contrast to other arrangements with greater depth of penetration such as ATR. The specular reflectance FT−IR spectra for the porphyrins were measured neat (by casting on silicon substrates) and bound to the TiO_2 thin films. All spectra were obtained using typically 500 scans with a

resolution of 4 cm^{-1}. The background was removed by subtracting the signal obtained from a gold substrate.

2.5. Gas Sensing. A gas testing chamber was used to expose the samples to the VOCs. This chamber consisted of a gas inlet and an outlet, a Peltier heating−cooling device and housings for two optical fibers that deliver and collect the light for the optical measurements. Further details regarding this setup can be found elsewhere.[23] The fibers were connected to a World Precision Instrument "Spectromate" spectrophotometer. Gaseous VOCs were obtained by bubbling dry nitrogen through a bottle immersed in a temperature-controlled water bath containing the desired neat liquid analyte. By means of this procedure, the resulting gas was composed by dry nitrogen saturated in each VOC, whose concentration can be calculated through its vapor pressure at the corresponding temperature. Vapor pressures were controlled by regulating the bath temperature, 20 °C in all cases except for the VOC concentration dependence experiments where a temperature of 0 °C was used in order to avoid a possible condensation of the analyte inside the gas chamber or the tubing system. Finally, the exact desired concentration was obtained by diluting the VOC−N_2 gas stream with another N_2 gas stream, and calculated by applying the corresponding dilution factor. Similar procedures for the generation of low ppm levels of VOCs in nitrogen can be found in the literature.[4]

Prior to the gas exposure phase, dry N_2 was introduced through the gas inlet to allow complete desorption of possible contaminating gases from the inner walls of the chamber and thus preventing the contamination of the samples. Then, the samples were introduced into the gas chamber and again dry N_2 was introduced into the chamber to allow complete desorption of possible contaminating gases adsorbed on the sample. After this, the gas mixture (VOC and N_2) was directed into the gas chamber until complete saturation of the porphyrin. All samples were exposed at room temperature (~293 K). For the recovery phase, dry N_2 was introduced again to remove all the VOC gases from the chamber. This phase occurred at elevated temperature (~383 K) to allow complete desorption of the VOCs from the samples.

2.6. Identification Patterns. To create selective easy-to-read identification patterns, we have developed an innovative way of showing the optical response based on imaging spectroscopy. For each porphyrin and analyte, the nonexposure spectrum was subtracted from the exposure one at each wavelength and then normalized to the maximum absorbance of the nonexposed spectrum. Finally, the resulting values were squared to maximize differences. All the squared difference spectra for each analyte in the Soret band region were put together and converted into an $m \times n$ matrix (where m is the wavelength and n is the number of used porphyrins, $n = 11$ in this case) which was represented as color image using Origin Pro 8 software. Through this representation, a barcodelike image consisting of 11 columns and m rows, in which the different values ($11 \times m$ pixels) are colored from red to blue (i.e., non change points are represented in red and maximum change points are colored in blue), was created for each analyte.

3. RESULTS AND DISCUSSION

3.1. TiO_2 Thin Film Microstructure. Cross−section and normal FESEM images corresponding to TiO_2 thin films prepared by GAPVD at an angle of deposition of 70° are shown in Figure 2. The cross-section image shows the tilt angle of the columns and the thickness of the film. The angle formed by the columns and the substrate was found to be 60° with a film thickness of approximately 350 nm.

The analysis of the images in Figure 2 reveals that the observed apertures correspond to mesopores (i.e., pores bigger than 2 nm) extending from the surface to the bottom of the film. This allows the accessibility of large molecules like porphyrins during the composite preparation and improves subsequent applications that would require a fast diffusion of gas molecules through the film structure.

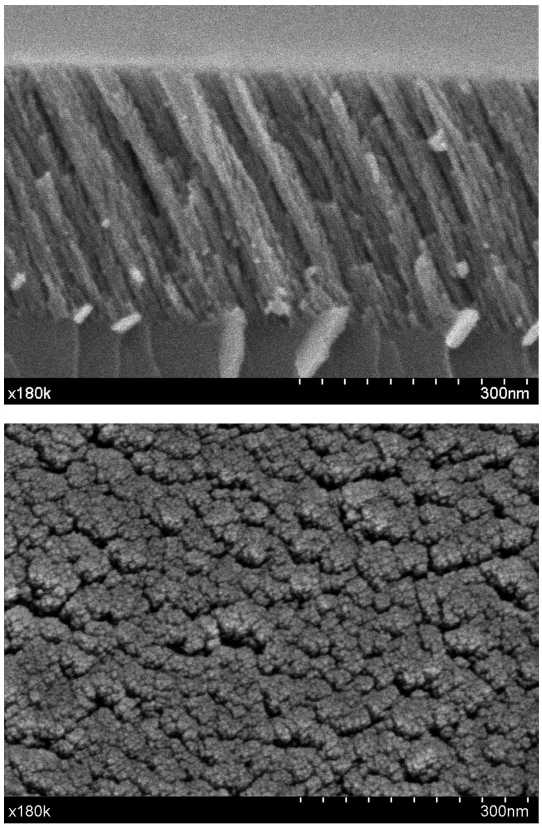

Figure 2. (Top) Cross-section and (bottom) planar FESEM images of the columnar TiO_2 thin films prepared at an angle of deposition of 70°.

The porosity of the TiO_2 thin films can also be deduced from the value of their refraction index, estimated as 1.79 from the recorded and simulated UV−visible transmission spectra respectively (data not shown). This value is much smaller than that corresponding to the bulk material (i.e., 2.49 for TiO_2 in the form of anatase) and is a clear proof of the high porosity of the film. The low refraction index makes these films very useful for UV−visible spectroscopy applications.

All different angles of incidence (60, 70, 80, 85, and 90°) showed similar properties, but in order to avoid any possible difference, all experiments were carried out using films of an angle of 70° as host material for the porphyrins. FESEM images of different films prepared with this angle were analyzed and the differences in thickness were no greater than 20 nm.

3.2. Binding to TiO_2. Specular reflectance FT−IR spectra of H_2TCPP and ZnTCPP neat and bound to TiO_2 are shown in Figure 3. In all cases, the existence of typical bands corresponding to the symmetric and asymmetric stretching modes of the pyrrole ring (ν (C−H), ν (C═C). and ν (C═N)) within the meso-tetraphenylporphyrin macrocycle was evident over the range 700−1500 cm^{-1}.[24] However, that which reveals the binding interaction between the TCPP and the metal oxide surface is the comparison of changes in the region of the carbonyl group in the FT−IR spectra. Neat samples of H_2TCPP and ZnTCPP showed a band in the region of 1685−1695 cm^{-1}, which is characteristic of the ν (C═O) stretch and a strong band in the 1385−1415 cm^{-1} region due to the ν (C−O) stretch of the carboxylic acid groups. It is worth mentioning that these bands are known to shift to lower frequencies in the case of the ν (C═O) stretch and to higher ones for the ν (C−

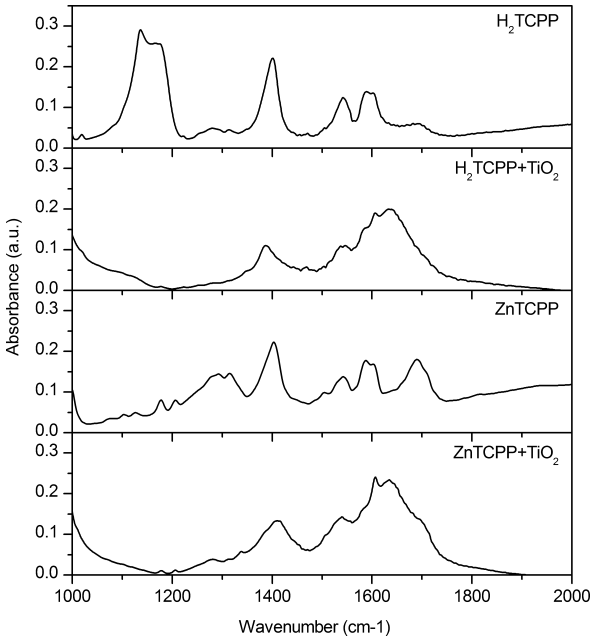

Figure 3. Specular reflectance FT−IR spectra of H_2TCPP and ZnTCPP neat (by casting on silicon substrates) and bound to TiO_2.

O) stretch due to extensive hydrogen bonding of the carboxylic acid groups in para-substituted TCPPs where the −COOH groups[25] are situated in the plane of the tetrapyrrole macrocycle.

Binding to TiO_2 colloidal films has been associated with the disappearance of the bands corresponding to the ν (C═O) and ν (C−O) stretching modes, and the appearance of strong and broad bands at ∼1400 cm^{-1} and ∼1550 cm^{-1} characteristic of the symmetric and asymmetric ν (CO_2^-) stretches respectively.[26] These spectral changes have been found to be compatible with chelating and/or bidentate binding modes of the carboxylate groups on the TiO_2 surface.[26−30]

In our case, the bands corresponding to the C═O and C−O stretching modes disappear only partially with a broadening of the latter, especially in the case of ZnTCPP/TiO_2, while the appearance of that of the symmetric ν (CO_2^-) stretch is not so evident due to overlapping with the remaining and shifted ν (C−O) stretch band. Moreover, the changes in the 1500−1750 cm^{-1} region are hindered in part by the presence of a strong and broad band around 1630 cm^{-1} corresponding to the TiO_2 in the columnar film. The IR spectrum of a porphyrin-free TiO_2 film is available in the Supporting Information (Figure S1).

The observed partial changes are therefore consistent with the presence of free carboxylic acid groups coexisting with carboxylate groups bound to TiO_2. In this situation, the para substituted TCPPs are likely to be bound only by one or two of its four carboxyl groups to the metal oxide surface due to its planar structure, resulting in a perpendicular orientation of the molecule with respect to the surface.[26,31] In fact, in smooth and even surfaces, the flat geometry of the dye molecule would not admit another type of binding, although we can also assume that the irregular surface of the columns in the titania film allows porphyrins to bind more than two carboxylate groups and hence we could find molecules with one to four points anchored to the titania surface. In any case, most of the dye molecules are only partially anchored to the TiO_2 with a perpendicular orientation with respect to the surface that allows them to interact (face to face) with other molecules causing aggregation.

UV−visible spectra of H_2TCPP in EtOH solution and bound to TiO_2 films are shown in Figure 4. In the solution spectrum,

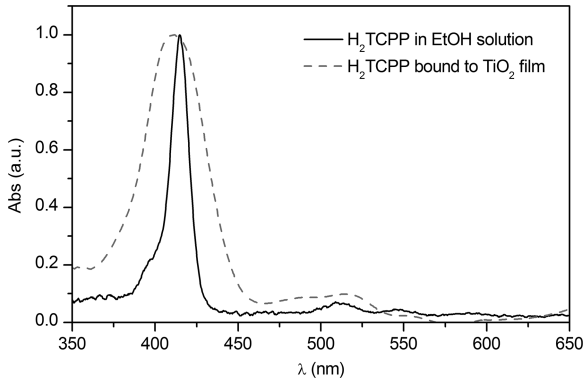

Figure 4. UV−visible absorption spectra of H_2TCPP in ethanol solution (solid line) and bound to a titania film (dashed line).

H_2TCPP appears in its monomeric form with the Soret band centered at 415 nm. However, the spectrum of the porphyrin in the film featured a broadening of the Soret band whose maximum is blue-shifted (5 nm) with respect to the solution. This behavior can be mainly attributed to the formation of H-aggregates (face-to-face stacking) between porphyrin molecules.,[26,32,33] although the formation of a certain number of J−-aggregates cannot be discarded.

The shifting and broadening of the absorption spectra of aggregated species in thin films, relative to the monomeric spectrum in solution, has been interpreted by the application of exciton models such as the point dipole model proposed by McRae and Kasha[34,35] or the extended dipole model proposed by Kuhn and collaborators.[36,37] Excellent discussions and comparisons between them can be found in the literature,[38−40] as well as examples of the application of these models to aggregated porphyrins when deposited as thin films.[41,42] According to the point dipole approximation, and assuming that the transition moments of the chromophores are lying parallel to each other, a red shift is expected when the displacement angle between the transition moments and the line connecting their centers is smaller than 54° (J-aggregate), whereas a larger displacement angle will produce a blue shift (H-aggregate). In general, a Scheibe aggregate[43,44] (J-aggregate) is formed when Coulomb attraction forces between the interacting dipoles outweigh repulsion. Often, this situation is predicted more accurately by the extended dipole approximation, especially at direct contact of the molecules.[11] In the case of the porphyrins studied here, the observed blue-shift in the UV−visible spectra reveals that the dyes form H-aggregates when anchored to the TiO_2 film. However, the broadening of the Soret band indicates that along with the H−aggregates and the monomers, there are also some J-aggregates present in the film.

This result is not surprising taking into account the porphyrin binding revealed by the IR experiments where only 1 or 2 of the 4 carboxylic groups are bound to the TiO_2 matrix. With this arrangement, where the porphyrin central ring is normal to the TiO_2 surface (vertical orientation), it is expected to observe these types of π−π interactions. Depending of the exact relative position of adjacent macrocycles, determined by

the anchoring site on the metal oxide surface, different types of aggregates (H or J) would be formed.

Although the porphyrin aggregation could be detrimental for its gas sensing application due to a hindered access of the analytes to the porphyrin coordination sites,[11] it will be shown that such $\pi-\pi$ interaction is not strong enough to avoid effective analyte binding probably due to the positive influence of the TiO_2 matrix whose chemical binding with the dye molecule prevents a closer position of their conjugated rings thus avoiding a higher degree of aggregation.

Although this spectroscopic characterization has been focused on the H_2TCPP and ZnTCPP derivatives, the rest of the metal complexes showed a similar behavior in terms of binding to TiO_2 and $\pi-\pi$ interaction.

In order to assess the dye surface coverage, the porphyrin surface concentration Γ, was calculated for the different derivatives by integrating the absorption spectrum, both in solution and in the film, according to the method provided elsewhere.[18] The Γ values were in the range $(3-5) \times 10^{-9}$ mol cm^{-2} depending on the porphyrin, with maximum variations below 10% of the average value in all cases.

3.3. Gas–Sensitive Optical Properties and Recognition Patterns. Composite porphyrin/TiO_2 films obtained from each one of the 11 porphyrins have been exposed to vapors of the following 12 different analytes: acetone, acetonitrile, chloroform, butylamine, dichloromethane, diethylether, dimethylformamide, ethanol, hexanethiol, hexylamine, methanol, and tetrahydrofuran. Figure 5 (top) shows the

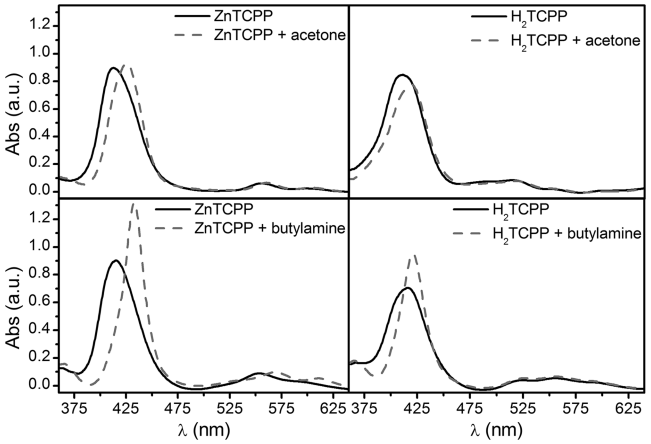

Figure 5. Top: Before (solid line) and after (dashed line) exposure to acetone spectra of ZnTCPP/TiO_2 (left) and H_2TCPP/TiO_2 (right) composite films. Bottom: Before (solid line) and after (dashed line) exposure to butylamine spectra of ZnTCPP (left) and H_2TCPP (right) films.

spectra of ZnTCPP and H_2TCPP composite films before and after their exposure to acetone. In the case of the ZnTCPP, the Soret band is red-shifted (13 nm) and increased after the exposure. The exposed H_2TCPP film spectrum shows less red shift (8.5 nm) and some decrease with respect to the pre–exposure spectrum. In Figure 5 (bottom), spectra of ZnTCPP and H_2TCPP films before and after exposure to butylamine are shown. In this case, the ZnTCPP Soret band is more red–shifted after the exposure than when exposed to acetone (17.5 nm), and the intensity of the absorbance is much more increased. However, the H_2TCPP spectrum shows a smaller shift (4.5 nm), and an intensity increase like in the case of the ZnTCPP derivative. The spectral changes of the rest of porphyrins upon exposure to all the analytes are available in the Supporting Information (Figure S2). In most cases, the spectral analysis showed significant differences of their respective spectral shifts and intensity changes when exposed to the different compounds. Through the recovery phase, samples returned to their original status. To explore the repeatability and reversibility of the system, we exposed all samples several times to each of the analytes and recovered them, showing no differences between cycles (data not shown).

On the other hand, the reproducibility of the response was evaluated in all cases by using the maximum variation in the absorbance change for at least 3 different films of the same porphyrin exposed to the same analyte (butylamine). The statistical analysis yielded a mean %RSD (relative standard deviation) for the response of 4.8% reaching a maximum value of 8.9% for MnTCPP. This good reproducibility is probably due to a complete saturation of the TiO_2 film by the infiltrated dye and the low variability in the film thickness.

The observed spectral changes demonstrate that porphyrins are a good choice for the detection of multiple analytes. In particular, the open coordination sites for axial ligation and the large spectral shifts upon ligand binding make the metalloporphyrins very appropriate for the detection of metal–ligating vapors,[43,44] although other type of chemical interactions such as Lewis or Brønsted acid–base interactions, hydrogen bonding, etc. are also possible. Moreover, the different response of the different porphyrins to each analyte reveals their potential use as selective sensors by using a proper combination of the corresponding responses.

A selective response can be obtained for each analyte through the analysis of the whole set of porphyrins, but owing to the large amount of collected information, a previous data processing stage is necessary in order to focus the attention on the spectral change.

A quantitative measure of the response is useful for a fast analysis which includes several porphyrins and analytes, even more in this work, where the number of different cases is elevated. A commonly used method comprises the subtraction of the gas exposure spectrum from the non–exposure one and the obtained difference at each wavelength is squared and then grouped in only one value by applying a summation function.[45] The drawback of this kind of quantification is the loss of information caused by summarizing a whole spectrum (or a difference spectrum) in a numerical value. The spectral changes are characterized not only by the spectral shift in terms of wavelength values but also by the corresponding intensity of the absorbance; this is the whole spectrum profile. Such changes have been shown to be characteristic of each porphyrin and analyte, and cannot be distinguished when changes in intensity and wavelength are represented as one value alone.

To reduce the loss of information, an innovative way of showing the response of all porphyrins to a certain analyte is shown in Figure 6. The resulting images possess spectral resolution and can be interpreted as recognition patterns for each analyte. Through these patterns, the shift and the change in absorbance intensity can be easily distinguished. By means of these images, like in the case of using bar codes, both the position and the intensity of the different bands give information about the compound to be identified. Each pattern consists of 11 columns corresponding to the 11 porphyrins used in this work. Every column shows the squared average difference of the post- and pre-exposure spectra in a color scale

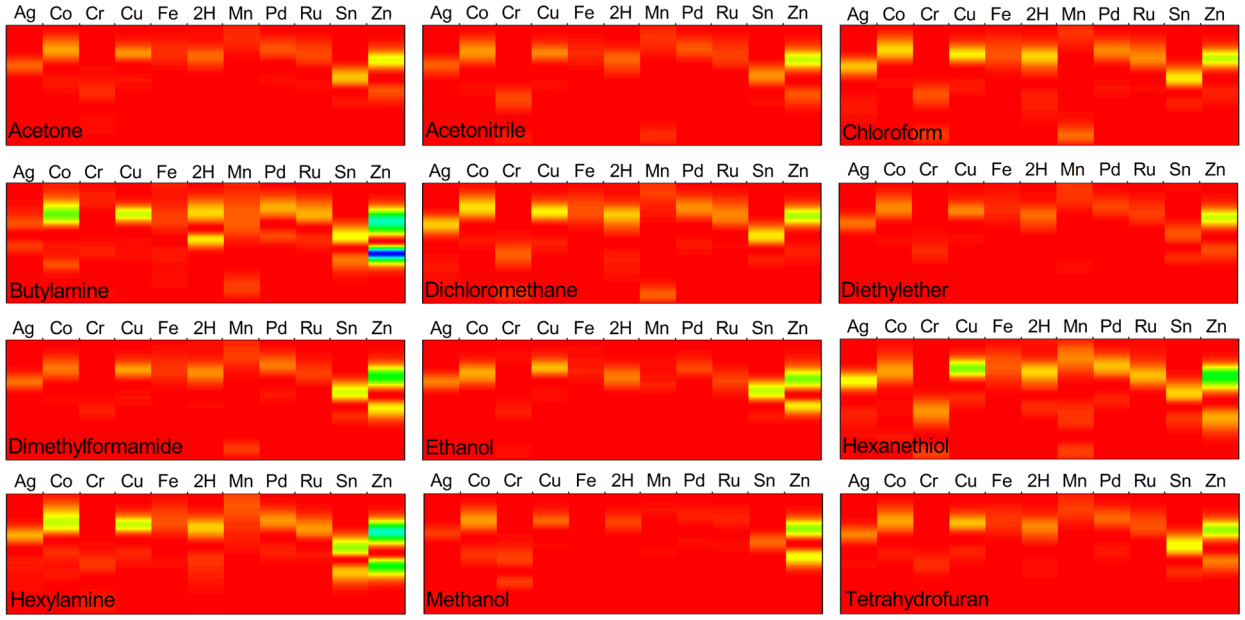

Figure 6. Identification patterns obtained for the different analytes. Color scale goes from red to blue, where red means no change between exposed and nonexposed spectra and blue is the highest change detected.

from red to blue, where red corresponds to no change between exposed and non−exposed spectra and blue is the highest change detected. As detailed in the Experimental Section, this method maintains all the information regarding the intensity changes at each wavelength of the Soret band region. Another interesting method found in the literature consists of a color RGB difference image of a spot of the porphyrin samples before and after exposure to the target analyte.[4] In that case, only 3 values related to the difference spectrum (red, green and blue of a 8-bit color palette) are used for the identification pattern. Although this method has shown excellent sensing capabilities in terms of selectivity and analyte discrimination[4,5,7,8] a possible loss of information regarding the spectral changes cannot be discarded since such spectral changes contain a potential identification value at each wavelength of the spectrum. Therefore, an image containing all these changes can be nowadays an ideal identification pattern given that cheap and versatile image-reading devices are available in the market. Additionally, the proposed approach is ready to access other spectral regimes such as the infrared, provided that new materials with sensing activity in that range are used, which enables this identification system to exploit optical sensing beyond the human-vision-based RGB colorimetric systems.

As can be seen in Figure 6, each analyte has a characteristic pattern that differs from the rest in one way or another, allowing the virtual identification of all analytes. Although some compounds show similarities to others, for example, acetone and acetonitrile or chloroform and dichloromethane have similar patterns, they are not identical.

In particular, butylamine, hexylamine, hexanethiol, and dimethylformamide are the analytes that produce the highest values of change, especially when the exposed porphyrin is ZnTCPP. On the other hand, the exposure to acetone or diethylether results in a low response. To further improve our discrimination capability, new strategies comprising the use of new porphyrin derivatives with more efficient structures are under study. Regarding the porphyrin behavior, ZnTCPP is by far the most responsive. Other derivatives, such as CrTCPP or FeTCPP, show low values of response. However, this cannot be considered a drawback since it is known that a highly selective odor sensing device (like the human olfactory system) must consist of a combination of highly responsive receptors with reduced selectivity and highly selective ones that usually show low response values.[46] At this point, it is worth mentioning that multiple gas sensing should be demonstrated before a wider range of real applications can be proposed. Nonetheless, single gas detection is possible with the proposed system and it capability for the analysis of mixtures in now under investigation.

A future integration of the sensing films into a sensor array would imply the use of a parallel multiple fiber-optic setup and a mechanical arrangement to measure sequential layers,[47] in such a way that the resulting identification images would be obtained in real time.

3.4. Concentration Dependence and Kinetics of the Gas Exposure and Recovery. The development of a sensor involves the search of some specific characteristics. A good sensor must be selective, and its response needs to be fast, reproducible, reversible, and concentration-dependent for quantification purposes.

The kinetics of the TCPPs/TiO_2 films response when exposed to the different VOCs was analyzed by following the time evolution of the absorbance at the wavelength of its maximum change. The ZnTCPP/TiO_2 film response to EtOH is provided as an example in Figure 7. This figure depicts a sequence of five consecutive EtOH gas exposure−recovery cycles of a ZnTCPP composite film in which the EtOH concentration has been increased after each recovery phase. These cycles were obtained by bubbling dry N_2 through liquid EtOH at a temperature of 0 °C and diluting the resulting gas stream with another N_2 stream in the appropriate proportion. As can be seen, increasing concentrations of EtOH result in an increase in the magnitude of response, indicating that the sensor behavior is concentration-dependent. Therefore, the system is also suitable to be used for quantification purposes. A wider concentration range was tested with identical results

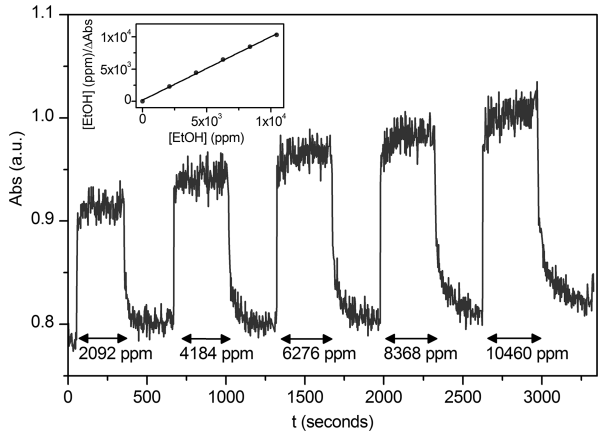

Figure 7. Kinetics of the exposure of a ZnTCPP composite film to EtOH gas at a wavelength of 430 nm. Inset: Langmuir adsorption plot for a ZnTCPP composite film.

down to ~100 ppm EtOH (see Figure S3 in the Supporting Information).

An evaluation of the concentration dependence of the response can be obtained by applying an isotherm model, which describes the adsorption/desorption equilibrium of the gas molecules onto the solid surface. The Langmuir adsorption isotherm[48] has been used to characterize the adsorption of many types of molecules onto different materials.[49−51] It is usually expressed by

$$\frac{n_{ads}}{N_S} = \frac{\lambda c}{1 + \lambda c} \quad (1)$$

where n_{ads} is the number of gas molecules adsorbed (which is proportional to the change in Soret band absorbance, ΔAbsorbance), N_s is the number of adsorption sites, λ is a constant relating to the adsorbability of the gas and c is the concentration of the gas, [EtOH]. Rearrangement of eq 1 leads to the linear form of the Langmuir adsorption isotherm

$$\left(\frac{c}{n_{ads}}\right) = \left(\frac{c}{N_S}\right) + \left(\frac{1}{N_S\lambda}\right) \quad (2)$$

Therefore, a plot of c/n_{ads} versus c should yield a straight line if the data points follow the Langmuir model. Figure 7 (inset) shows a plot of c/ΔAbsorbance vs c, and a straight line is obtained, indicating that Langmuir adsorption, even with its limited assumptions, provides a basic understanding of the EtOH−ZnTCPP interaction during the sensing process. According to the assumptions of the Langmuir model, it can be concluded that the activation energy of adsorption is the same for all binding sites in the thin film assembly, that there are a fixed number of localized surface sites present on the surface and that EtOH molecules striking a surface site that is already occupied do not adsorb.

The Langmuir adsorption model was applied to the exposure of all TCPPs/TiO_2 films to butylamine gas and to the exposure of ZnTCPP/TiO_2 films to all 12 used analytes (see Tables S1 and S2 in the Supporting Information). In all cases, a straight line was obtained, indicating that our system follows the Langmuir model.

To know quantitatively the speed of response, the value of t_{50}, which is the time taken for the absorbance to reach the 50% of its total maximum change, was calculated. In the case of the ZnTCPP/TiO_2 film response to EtOH, the obtained value was approximately 4.5 s in all cycles, revealing a very fast response process. As for the Langmuir model, t_{50} was calculated for the exposure of all TCPPs/TiO_2 films to butylamine gas and to the exposure of ZnTCPP/TiO_2 films to all 12 used analytes (see Tables S1 and S2 in the Supporting Information). In all cases, the response was found to be very fast ($t_{50} \approx 4-9$ s). Such behavior can be attributed to two probable reasons. On the one hand, the speed of the response is related directly to the sensitivity of the used porphyrins. On the other hand, the properties of the titania film play an important role. The microstructured film is highly porous, which leads to an easy diffusion of the gas molecules through the surface and therefore every porphyrin is exposed to the analyte without any delay.

Overall, the set of porphyrins have shown good capabilities for gas sensing with interesting odor detection applications. The response has been found to be very selective, allowing the identification of the different analytes. Also, the composite porphyrin/TiO_2 films have yielded fast and concentration-dependent responses, making the quantification of the volatile compounds possible through calibration curves based on the Langmuir isotherm.

4. CONCLUSIONS

Microstructured columnar TiO_2 thin films prepared by GAPVD have been used as host materials of several porphyrins. These films are non−dispersive and hence appropriate for UV−visible spectroscopy. Also, its porous microstructure allows gas diffusion through the film, making them suitable for gas sensing.

Several porphyrins, featuring carboxylic groups that allow chemical binding to titania, have been bound to the columnar TiO_2 thin films and exposed to a wide range of volatile compounds. When hosted in the film, the porphyrins featured a blue shift and broadening of the Soret band, which has been attributed to the formation of H−aggregates (face-to-face stacking) between porphyrin molecules.

The gas-sensitive properties of the composite films have been studied, showing a good selectivity to the analyzed volatile compounds. For each analyte, an image−like identification pattern based on spectral imaging has been obtained, which facilitates the straightforward recognition of every compound. The responses were found to be concentration dependent, allowing analyte quantification through calibration curves. The kinetics of the exposure to several analytes showed a fast response, with a value of t_{50} of a few seconds, which arises from both the sensitivity of the porphyrins and the high porosity of the TiO_2 films. Although the system has not yet been tested with mixed gases, it has been proven to be valid for the identification and quantification of individual VOCs.

■ ASSOCIATED CONTENT

Supporting Information

Specular reflectance FT−IR spectrum of a TiO2 film. UV−visible spectra of AgTCPP/TiO_2, CoTCPP/TiO_2, CuTCPP/TiO_2, CrTCPP/TiO_2, FeTCPP/TiO_2, H_2TCPP/TiO_2, MnTCPP/TiO_2, PdTCPP/TiO_2, RuTCPP/TiO_2, SnTCPP/TiO_2 and ZnTCPP/TiO_2 composite films before and after their exposure to acetone, acetonitrile, chloroform, butylamine, dichloromethane, diethylether, dimethylformamide, ethanol, hexanethiol, hexylamine, methanol, and tetrahydrofuran. Kinetics of the exposure of a ZnTCPP composite film to EtOH gas at a wavelength of 430 nm. Langmuir adsorption model results and t_{50} for the exposure of all TCPPs/TiO_2 films

to butylamine gas and for the exposure of ZnTCPP/TiO_2 films to all 12 used analytes. This material is available free of charge via the Internet at http://pubs.acs.org.

AUTHOR INFORMATION

Corresponding Author

*E-mail: jmpedpoy@upo.es.

Notes

The authors declare no competing financial interest.

ACKNOWLEDGMENTS

We thank the Ministry of Science and Education of Spain (Projects PET2007_0363_01/_02 and TEC2010-21830-C02-01) and the Junta de Andalucía (Project TEP-5283) for financial support.

REFERENCES

(1) Albert, K. J.; Lewis, N. S.; Schauer, C. L.; Sotzing, G. A.; Stitzel, S. E.; Vaid, T. P.; Walt, D. R. *Chem. Rev.* **2000**, *100*, 2595−2626.

(2) Gardner, J. W.; Bartlett, B. N. In *Electronic Noses: Principles and Applications*; Oxford University Press: New York, 1999.

(3) Rakow, N. A.; Sen, A.; Janzen, M. C.; Ponder, J. B.; Suslick, K. S. *Angew. Chem., Int. Ed.* **2005**, *44*, 4528−4532.

(4) Rakow, N. A.; Suslick, K. S. *Nature* **2000**, *406*, 710−713.

(5) Suslick, K. S. *MRS Bull.* **2004**, *29*, 720−725 +702.

(6) Suslick, K. S.; Rakow, N. A.; Sen, A. *Tetrahedron* **2004**, *60*, 11133−11138.

(7) Suslick, K. S.; Bailey, D. P.; Ingison, C. K.; Janzen, M.; Kosal, M. E.; McNamara, W. B., III; Rakow, N. A.; Sen, A.; Weaver, J. J.; Wilson, J. B.; Zhang, C.; Nakagaki, S. *Quim. Nova.* **2007**, *30*, 677−681.

(8) Lim, S. H.; Feng, L.; Kemling, J. W.; Musto, C. J.; Suslick, K. S. *Nature Chem.* **2009**, *1*, 562−567.

(9) Feng, L.; Musto, C. J.; Kemling, J. W.; Lim, S. H.; Zhong, W.; Suslick, K. S. *Anal. Chem.* **2010**, *82*, 9433−9440.

(10) Di Natale, C.; Paolesse, R.; D'Amico, A. *Sens. Actuators, B* **2007**, *121*, 238−246.

(11) Pedrosa, J. M.; Dooling, C. M.; Richardson, T. H.; Hyde, R. K.; Hunter, C. A.; Martín, M. T.; Camacho, L. *Langmuir* **2002**, *18*, 7594−7601.

(12) Pedrosa, J. M.; Dooling, C. M.; Richardson, T. H.; Hyde, R. K.; Hunter, C. A.; Martín, M. T.; Camacho, L. *J. Mater. Chem.* **2002**, *12*, 2659−2664.

(13) De Miguel, G.; Martín-Romero, M. T.; Pedrosa, J. M.; Muñoz, E.; Pérez-Morales, M.; Richardson, T. H.; Camacho, L. *J. Mater. Chem.* **2007**, *17*, 2914−2920.

(14) Roales, J.; Pedrosa, J. M.; Castillero, P.; Cano, M.; Richardson, T. H. *Thin Solid Films* **2011**, *519*, 2025−2030.

(15) Campbell, W. M.; Burrell, A. K.; Officer, D. L.; Jolley, K. W. *Coord. Chem. Rev.* **2004**, *248*, 1363−1379.

(16) Borrás, A.; Barranco, A.; González-Elipe, A. R. *J. Mater. Sci.* **2006**, *41*, 5220−5226.

(17) Sánchez-Valencia, J. R.; Borrás, A.; Barranco, A.; Rico, V. J.; Espinos, J. P.; González-Elipe, A. R. *Langmuir* **2008**, *24*, 9460−9469.

(18) Castillero, P.; Sánchez-Valencia, J. R.; Cano, M.; Pedrosa, J. M.; Roales, J.; Barranco, A.; González-Elipe, A. R. *ACS Appl. Mater. Interfaces* **2010**, *2*, 712−721.

(19) Cano, M.; Castillero, P.; Roales, J.; Pedrosa, J. M.; Brittle, S.; Richardson, T.; González-Elipe, A. R.; Barranco, A. *Sens. Actuators, B* **2010**, *150*, 764−769.

(20) Özgür, Ü.; Alivov, Y. I.; Liu, C.; Teke, A.; Reshchikov, M. A.; Doğan, S.; Avrutin, V.; Cho, S.; Morko, H. *J. Appl. Phys.* **2005**, *98*, 1−103.

(21) Lim, S. H.; Kemling, J. W.; Feng, L.; Suslick, K. S. *Analyst* **2009**, *134*, 2453−2457.

(22) Sivalingam, Y.; Martinelli, E.; Catini, A.; Magna, G.; Pomarico, G.; Basoli, F.; Paolesse, R.; Di Natale, C. *J. Phys. Chem. C* **2012**, *116*, 9151−9157.

(23) Dooling, C. M.; Worsfold, O.; Richardson, T. H.; Tregonning, R.; Vysotsky, M. O.; Hunter, C. A.; Kato, K.; Shinbo, K.; Kaneko, F. *J. Mater. Chem.* **2001**, *11*, 392−398.

(24) Long, B.; Nikitin, K.; Fitzmaurice, D. *J. Am. Chem. Soc.* **2003**, *125*, 5152−5160.

(25) Galoppini, E.; Rochford, J.; Chen, H.; Saraf, G.; Lu, Y.; Hagfeldt, A.; Boschloo, G. *J. Phys. Chem. B* **2006**, *110*, 16139−16161.

(26) Rochford, J.; Chu, D.; Hagfeldt, A.; Galoppini, E. *J. Am. Chem. Soc.* **2007**, *129*, 4655−4665.

(27) Deacon, G. B.; Phillips, R. J. *Coord. Chem. Rev.* **1980**, *33*, 227−250.

(28) Finnie, K. S.; Bartlett, J. R.; Woolfrey, J. L. *Langmuir* **1998**, *14*, 2741−2749.

(29) Vittadini, A.; Selloni, A.; Rotzinger, F. P.; Grätzel, M. *J. Phys. Chem. B* **2000**, *104*, 1300−1306.

(30) Nazeeruddin, M. K.; Humphry-Baker, R.; Liska, P.; Grätzel, M. *J. Phys. Chem. B* **2003**, *107*, 8981−8987.

(31) Rochford, J.; Galoppini, E. *Langmuir* **2008**, *24*, 5366−5374.

(32) Aratani, N.; Osuka, A.; Cho, H. S.; Kim, D. *J. Photochem. Photobiol., C* **2002**, *3*, 25−52.

(33) Choi, M. *Tetrahedron Lett.* **2008**, *49*, 7050−7053.

(34) Mcrae, E. G.; Kasha, M. *J. Chem. Phys.* **1958**, *28*, 721−722.

(35) McRae, E. G.; Kasha, M. In *Physical Processes in Radiation Biology*; Academic Press; New York, 1964; pp 23−42.

(36) Czikklely, V.; Forsterling, H. D.; Kuhn, H. *Chem. Phys. Lett.* **1970**, *6*, 207−210.

(37) Kuhn, H.; Foersterling, H. In *Principles of Physical Chemistry*; John Wiley & Sons: New York, 2000.

(38) Czikkely, V.; Försterling, H. D.; Kuhn, H. *Chem. Phys. Lett.* **1970**, *6*, 11−14.

(39) Evans, C. E.; Song, Q.; Bohn, P. W. *J. Phys. Chem.* **1993**, *97*, 12302−12308.

(40) Kuhn, H. *Colloids Surf., A* **2000**, *171*, 3−12.

(41) Schick, G. A.; Schreiman, I. C.; Wagner, R. W.; Lindsey, J. S.; Bocian, D. F. *J. Am. Chem. Soc.* **1989**, *111*, 1344−1350.

(42) Prieto, I.; Pedrosa, J. M.; Martín-Romero, M. T.; Möbius, D.; Camacho, L. *J. Phys. Chem. B* **2000**, *104*, 9966−9972.

(43) Scheibe, G. *Angew. Chem.* **1937**, *50*, 51−52.

(44) Kuhn, H.; Kuhn, C. *J. Aggregates* **1996**, 1−40.

(45) Dunbar, A. D. F.; Richardson, T. H.; McNaughton, A. J.; Hutchinson, J.; Hunter, C. A. *J. Phys. Chem. B* **2006**, *110*, 16646−16651.

(46) Röck, F.; Barsan, N.; Weimar, U. *Chem. Rev.* **2008**, *108*, 705−725.

(47) Di Natale, C.; Mignani, A. G.; Paolesse, R.; Macagnano, A.; Mencaglia, A. A.; D'Amico, A. *IEEE Sens. J.* **2005**, *5*, 1165−1173.

(48) Langmuir, I. *J. Am. Chem. Soc.* **1918**, *40*, 1361−1403.

(49) Worsfold, O.; Dooling, C. M.; Richardson, T. H.; Vysotsky, M. O.; Tregonning, R.; Hunter, C. A.; Malins, C. *J. Mater. Chem.* **2001**, *11*, 399−403.

(50) Chague, B.; Germain, J. P.; Maleysson, C.; Robert, H. *Sens. Actuators* **1985**, *7*, 199−207.

(51) Goldberg, S. *Plant Soil* **1997**, *193*, 35−48.